Prediction of Largest Peak Seismic Response at Flexible-Side Frame of Asymmetric Buildings

K.Fujii
Chiba Instutute of Technology,Japan

ABSTRACT:
In this present article, the modified procedure to predict the largest peak seismic response at flexible-side frame of asymmetric building considering horizontal bi-directional ground motion act in arbitrary angle of incidence is proposed. In the proposed procedure, two assumptions are made as follows; a) the major horizontal component of ground motion act in the direction of the principal axis of the first modal response, while the minor horizontal component of ground motion act in the direction perpendicular to the principal axis of the first modal response, b) the peak response of the first mode can be predicted from the major component of ground motion, while the peak response of the second mode can be predicted from the minor component of ground motion.
Two of four-story asymmetric buildings are investigated as application example. The results show the largest peak response at flexible-side frame can be satisfactorily predicted by the proposed procedure.

Keywords: asymmetric buildings, bi-directional excitation, pushover analysis, direction of seismic input

1. INTRODUCTION

It is well accepted that asymmetric buildings are vulnerable to earthquakes. This is because the excessive deformation may occur at the flexible and/or weak side frame due to the unfavorable torsional effect. That may lead to the premature failure of brittle members and finally collapse of whole buildings. For the seismic assessment of asymmetric building, it is essential to carry out 3-dimensional analysis considering the all possible direction of seismic input. However it is very time-consuming task to evaluate seismic response under all possible seismic intensity by incremental dynamic analysis (IDA) (Vanvasikos and Cornell, 2002) for all possible directions of seismic input, because the horizontal ground motion may act in any horizontal direction. Another approach for the seismic assessment of asymmetric building would be the evaluation of seismic response for critical direction of seismic input, which would produce the maximum response. Dolšek and Fajfar proposed a simplified performance assessment procedure for asymmetric buildings (Dolšek and Fajfar, 2007). In this procedure, seismic performance of asymmetric building is assessed based on pushover analysis in each of main orthogonal axis of building. However, since the critical direction of seismic input may not coincide with the main orthogonal axis of buildings; it may depends on the nonlinear structural characteristics and also characteristics of seismic inputs. The author has already proposed a simplified procedure to predict the largest peak displacement at flexible-side frame considering the critical direction of seismic input at each nonlinear stage (Fujii, 2010). However, only one-component horizontal ground motion is considered in the procedure proposed previously, and therefore the modification of this procedure to consider the bi-directional horizontal ground motion is needed.

In this article, the modified procedure to predict the largest peak seismic response at flexible-side frame of asymmetric building considering horizontal bi-directional ground motion act in arbitrary angle of incidence is proposed. In the numerical example, the nonlinear time-history analyses of four-story reinforced concrete asymmetric frame buildings under various directions of seismic inputs are carried out and compared with predicted results.

2. DESCRIPTION OF PROPOSED PROCEDURE

2.1. Concept of Proposed Procedure

The concept of the proposed procedure is shown in Fig. 2.1. As shown in this figure, a set of orthogonal U-V axis in X-Y plane is considered in this paper, and U-axis is taken as the principal axis of the first modal response, which is discussed by the author (Fujii, 2010 and 2011). Since the asymmetric buildings considering in this paper are *N*-Story buildings, 3*N* degrees of freedoms (3*N*-DOFs) are oriented for the multi-storey model studied herein. It is assumed that, when the largest peak response at flexible-side frame of asymmetric building occurs, the major horizontal component of ground motion act in the direction of the principal axis of the first modal response (U-axis), while the minor horizontal component of ground motion act in the direction perpendicular to the principal axis of the first modal response (V-axis). The largest peak response of the first mode is obtained from the equivalent single-degree-of-freedom (SDOF) model subjected to the major component of ground motion, and the peak response of second mode is obtained from the equivalent SDOF model subjected to minor component. The prediction of the largest peak response at flexible-side frame is based on a set of pushover analyses considering the combination of the two modal responses.

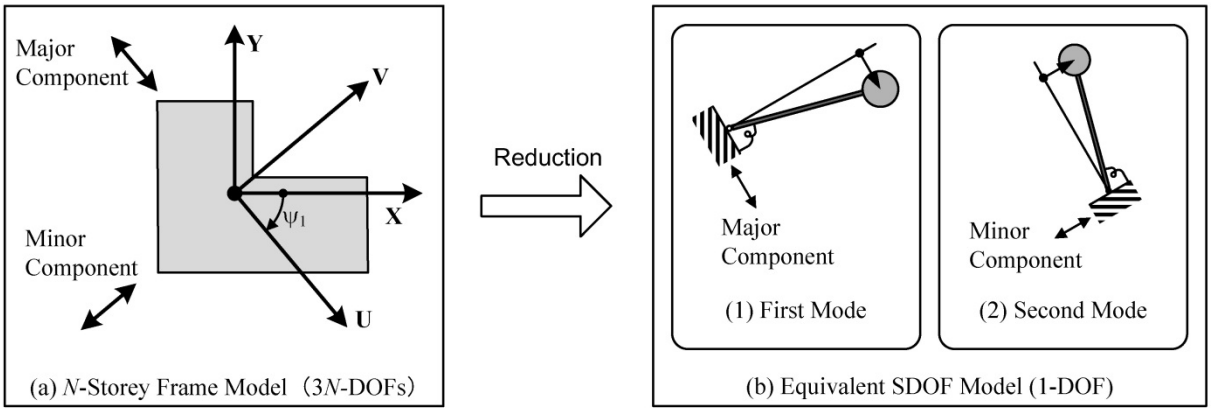

Figure 2.1 Concept of the proposed procedure

2.2. Outline of Proposed Procedure

The proposed procedure consists of following 5 steps:

STEP 1: Pushover analysis of asymmetric building model (first mode)
STEP 2: Estimation of seismic demand of equivalent SDOF model (first mode)
STEP 3: Pushover analysis of asymmetric building model (second mode)
STEP 4: Estimation of seismic demand of equivalent SDOF model (second mode)
STEP 5: Estimation of largest peak response at flexible-side frame

Note that the formulations of equivalent SDOF model and the derivation of the principal axis of the first modal response can be found in the previous articles (Fujii, 2010 and 2011).

2.2.1. STEP 1: Pushover Analysis of Asymmetric Building Model (First Mode)
The equivalent SDOF model for the first modal response is shown in Fig. 2.2. It is assumed that the major component of ground motion act in the direction of the principal direction of the first modal response at each nonlinear stage. The nonlinear properties of equivalent SDOF model, the equivalent acceleration A_{1U}^{*} − equivalent displacement D_{1U}^{*} relationship, which is referred to as the capacity curve, is determined based on the pushover analysis considering the change of the first mode shape at each nonlinear stage.

In the present article, “the displacement-based mode-adaptive pushover analysis”, which is proposed

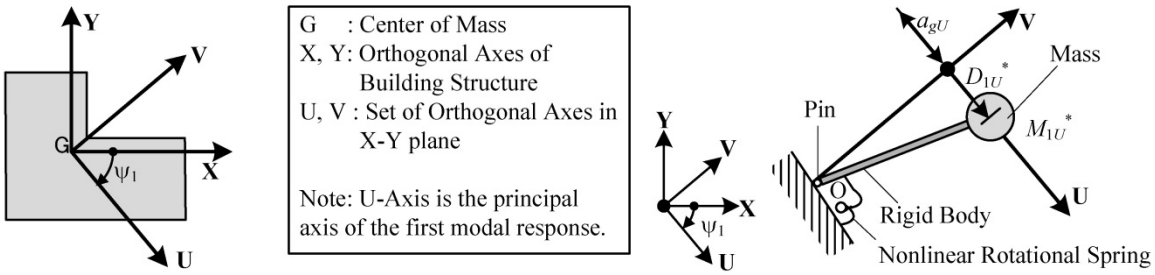

(a) Plan of Asymmetric Building Structure (b) Equivalent SDOF Model

Figure 2.2 Equivalent SDOF model (First Mode)

by the author (Fujii, 2010), is applied. This pushover analysis is based on the following assumptions.

1) All beams, columns and structural wall are modelled as as one-component models with two nonlinear flexural springs and rigid zones at both ends and one nonlinear shear spring at the middle of line element. The envelope curve of each nonlinear spring of members is symmetric in positive and negative range.
2) The equivalent stiffness of each nonlinear spring can be defined by their secant stiffness at peak deformation previously experienced in the calculation.
3) The first mode shape at each loading stage ${}_{\mathbf{n}}\boldsymbol{\varphi}_{\mathbf{1}} = \{ {}_n\phi_{X11} \cdots {}_n\phi_{XN1} \quad {}_n\phi_{Y11} \cdots {}_n\phi_{YN1} \quad {}_n\phi_{\Theta 11} \cdots {}_n\phi_{\Theta N1} \}^{\mathrm{T}}$ can be determined based on the equivalent stiffness.
4) The deformation shape imposed on a model is same as the first mode shape obtained in 2) and 3).

The equivalent acceleration and equivalent displacement at each loading stage, ${}_nA_{1U}{}^*$ and ${}_nD_{1U}{}^*$, are determined from Eqs. (2.1) and (2.2), respectively, assuming that displacement vector ${}_{\mathbf{n}}\mathbf{d}$ is proportional to the first mode vector at each nonlinear stage ${}_n\Gamma_{1U}\,{}_{\mathbf{n}}\boldsymbol{\varphi}_{\mathbf{1}}$.

$$ {}_nD_{1U}{}^* = \frac{{}_n\Gamma_{1U}\,{}_{\mathbf{n}}\boldsymbol{\varphi}_{\mathbf{1}}{}^{\mathrm{T}}\mathbf{M}_{\mathbf{n}}\mathbf{d}}{{}_nM_{1U}{}^*} = \frac{\sum_j \left(m_j\,{}_nx_j{}^2 + m_j\,{}_ny_j{}^2 + I_j\,{}_n\theta_j{}^2 \right)}{\sqrt{\left(\sum_j m_j\,{}_nx_j \right)^2 + \left(\sum_j m_j\,{}_ny_j \right)^2}} \tag{2.1} $$

$$ {}_nA_{1U}{}^* = \frac{{}_n\Gamma_{1U}\,{}_{\mathbf{n}}\boldsymbol{\varphi}_{\mathbf{1}}{}^{\mathrm{T}}\,{}_{\mathbf{n}}\mathbf{f}_{\mathbf{R}}}{{}_nM_{1U}{}^*} = \frac{\sum_j \left({}_nf_{RXj}\,{}_nx_j + {}_nf_{RYj}\,{}_ny_j + {}_nf_{MZj}\,{}_n\theta_j \right)}{\sqrt{\left(\sum_j m_j\,{}_nx_j \right)^2 + \left(\sum_j m_j\,{}_ny_j \right)^2}} \tag{2.2} $$

$$ {}_nM_{1U}{}^* = {}_n\Gamma_{1U}{}^2\,{}_{\mathbf{n}}\boldsymbol{\varphi}_{\mathbf{1}}{}^{\mathrm{T}}\mathbf{M}_{\mathbf{n}}\boldsymbol{\varphi}_{\mathbf{1}} = \frac{\left(\sum_j m_j\,{}_nx_j \right)^2 + \left(\sum_j m_j\,{}_ny_j \right)^2}{\sum_j m_j\,{}_nx_j{}^2 + \sum_j m_j\,{}_ny_j{}^2 + \sum_j I_j\,{}_n\theta_j{}^2} \tag{2.3} $$

$$ {}_n\Gamma_{1U} = \frac{{}_{\mathbf{n}}\boldsymbol{\varphi}_{\mathbf{1}}{}^{\mathrm{T}}\mathbf{M}_{\mathbf{n}}\boldsymbol{\alpha}_{\mathbf{U}}}{{}_{\mathbf{n}}\boldsymbol{\varphi}_{\mathbf{1}}{}^{\mathrm{T}}\mathbf{M}_{\mathbf{n}}\boldsymbol{\varphi}_{\mathbf{1}}} = \frac{\sqrt{\left(\sum_j m_j\,{}_nx_j \right)^2 + \left(\sum_j m_j\,{}_ny_j \right)^2}}{\sum_j m_j\,{}_nx_j{}^2 + \sum_j m_j\,{}_ny_j{}^2 + \sum_j I_j\,{}_n\theta_j{}^2} \tag{2.4} $$

$$ \mathbf{M} = \begin{bmatrix} \mathbf{M_0} & \mathbf{0} & \mathbf{0} \\ \mathbf{0} & \mathbf{M_0} & \mathbf{0} \\ \mathbf{0} & \mathbf{0} & \mathbf{I_0} \end{bmatrix}, \mathbf{M_0} = \begin{bmatrix} m_1 & & 0 \\ & \ddots & \\ 0 & & m_N \end{bmatrix}, \mathbf{I_0} = \begin{bmatrix} I_1 & & 0 \\ & \ddots & \\ 0 & & I_N \end{bmatrix} \tag{2.5} $$

$$\begin{cases} {}_{\mathbf{n}}\mathbf{d} = \{ {}_n x_1 \cdots {}_n x_N \quad {}_n y_1 \cdots {}_n y_N \quad {}_n \theta_1 \cdots {}_n \theta_N \}^{\mathbf{T}} \\ {}_{\mathbf{n}}\mathbf{f_R} = \{ {}_n f_{RX1} \cdots {}_n f_{RXN} \quad {}_n f_{RY1} \cdots {}_n f_{RYN} \quad {}_n f_{MZ1} \cdots {}_n f_{MZN} \}^{\mathbf{T}} \\ {}_{\mathbf{n}}\boldsymbol{\alpha}_{\mathbf{U}} = \{ \cos {}_n\psi_1 \cdots \cos {}_n\psi_1 \quad -\sin {}_n\psi_1 \cdots -\sin {}_n\psi_1 \quad 0 \cdots 0 \}^{\mathbf{T}} \end{cases} \tag{2.6}$$

$$\cos {}_n\psi_1 = \frac{\sum_j m_j {}_n\phi_{Xj1}}{\sqrt{\left(\sum_j m_j {}_n\phi_{Xj1}\right)^2 + \left(\sum_j m_j {}_n\phi_{Yj1}\right)^2}} = \frac{\sum_j m_j {}_n x_j}{\sqrt{\left(\sum_j m_j {}_n x_j\right)^2 + \left(\sum_j m_j {}_n y_j\right)^2}} \tag{2.7}$$

$$\sin {}_n\psi_1 = -\frac{\sum_j m_j {}_n\phi_{Yj1}}{\sqrt{\left(\sum_j m_j {}_n\phi_{Xj1}\right)^2 + \left(\sum_j m_j {}_n\phi_{Yj1}\right)^2}} = -\frac{\sum_j m_j {}_n y_j}{\sqrt{\left(\sum_j m_j {}_n x_j\right)^2 + \left(\sum_j m_j {}_n y_j\right)^2}} \tag{2.8}$$

In Eqs. (2.1) ~ (2.5), m_j and I_j are mass and moment of inertia of j-th floor, respectively, ${}_nM_{1U}{}^*$ and ${}_n\psi_1$ are the equivalent first modal mass with respect to U-axis at each nonlinear stage and the angle of incidence of principal axis of U-axis at each nonlinear stage, respectively. It should be noted that the reference axis considering the first mode response (U-axis) is displacement-dependent; it changes at each nonlinear stage as the first mode vector changes.

2.2.2. STEP 2: Estimation of seismic demand of equivalent SDOF model (first mode)

The largest peak equivalent displacement $D_{1U}{}^*{}_{\max}$ and the equivalent acceleration $A_{1U}{}^*{}_{\max}$ are obtained by using the equivalent linearization technique (Otani, 2000). In this step, it is assumed that the equivalent SDOF model representing the first mode response is subjected to the major component of ground motion.

2.2.3. STEP 3: Pushover Analysis of Asymmetric Building Model (Second Mode)

From the results of STEP 1 and STEP 2, the first mode vector corresponds to $D_{1U}{}^*{}_{\max}$, $\Gamma_{1Uie}\boldsymbol{\varphi}_{\mathbf{1ie}}$, is obtained and the second mode vector, $\Gamma_{2Vie}\boldsymbol{\varphi}_{\mathbf{2ie}}$, is determined from Eq. (2.9), in term of $\boldsymbol{\varphi}_{\mathbf{1ie}}$ and the second mode vector in elastic range $\boldsymbol{\varphi}_{\mathbf{2e}}$, considering the orthogonal condition of the mode vector.

$$\Gamma_{2Vie} = \frac{\boldsymbol{\varphi}_{\mathbf{2ie}}{}^{\mathbf{T}}\mathbf{M}\boldsymbol{\alpha}_{\mathbf{Vie}}}{\boldsymbol{\varphi}_{\mathbf{2ie}}{}^{\mathbf{T}}\mathbf{M}\boldsymbol{\varphi}_{\mathbf{2ie}}}, \boldsymbol{\varphi}_{\mathbf{2ie}} = \boldsymbol{\varphi}_{\mathbf{2e}} - \frac{\boldsymbol{\varphi}_{\mathbf{1ie}}{}^{\mathbf{T}}\mathbf{M}\boldsymbol{\varphi}_{\mathbf{2e}}}{\boldsymbol{\varphi}_{\mathbf{1ie}}{}^{\mathbf{T}}\mathbf{M}\boldsymbol{\varphi}_{\mathbf{1ie}}} \cdot \boldsymbol{\varphi}_{\mathbf{1ie}} \tag{2.9}$$

$$\boldsymbol{\alpha}_{\mathbf{Vie}} = \{ \sin\psi_{1ie} \cdots \sin\psi_{1ie} \quad \cos\psi_{1ie} \cdots \cos\psi_{1ie} \quad 0 \cdots 0 \}^{\mathbf{T}} \tag{2.10}$$

$$\cos\psi_{1ie} = \frac{\sum_j m_j \phi_{Xj1ie}}{\sqrt{\left(\sum_j m_j \phi_{Xj1ie}\right)^2 + \left(\sum_j m_j \phi_{Yj1ie}\right)^2}}, \sin\psi_{1ie} = -\frac{\sum_j m_j \phi_{Yj1ie}}{\sqrt{\left(\sum_j m_j \phi_{Xj1ie}\right)^2 + \left(\sum_j m_j \phi_{Yj1ie}\right)^2}} \tag{2.11}$$

Then another pushover analysis is carried out to obtain the force-displacement relationship representing the second mode response by applying the invariant force distribution $\mathbf{p_2}$ determined by Eq. (2.12).

$$\mathbf{p_2} = \mathbf{M}\left(\Gamma_{2Vie}\boldsymbol{\varphi}_{\mathbf{2ie}}\right) \tag{2.12}$$

The equivalent acceleration ${}_nA_{2V}{}^*$ and equivalent displacement ${}_nD_{2V}{}^*$ of equivalent SDOF model, representing the second mode response at each loading stage, are determined from Eq. (2.13).

$$ {}_nD_{2V}{}^{*} = \frac{\Gamma_{2Vie}\boldsymbol{\varphi}_{\mathbf{2ie}}{}^{\mathrm{T}}\mathbf{M}_{\mathbf{n}}\mathbf{d}}{M_{2Vie}{}^{*}}, {}_nA_{2V}{}^{*} = \frac{\Gamma_{2Vie}\boldsymbol{\varphi}_{\mathbf{2ie}}{}^{\mathrm{T}}{}_{\mathbf{n}}\mathbf{f}_{\mathbf{R}}}{M_{2Vie}{}^{*}}, M_{2Vie}{}^{*} = \Gamma_{2Vie}{}^{2}\boldsymbol{\varphi}_{\mathbf{2ie}}{}^{\mathrm{T}}\mathbf{M}\boldsymbol{\varphi}_{\mathbf{2ie}} \tag{2.13} $$

2.2.4. STEP 4: Estimation of seismic demand of equivalent SDOF model (second mode)
The seismic demand $D_{2V}{}^{*}{}_{\max}$ and $A_{2V}{}^{*}{}_{\max}$ of equivalent SDOF model is obtained by using the equivalent linearization technique, as discussed in Step 2. In this step, it is assumed that the equivalent SDOF model representing the second mode response is subjected to the minor component of ground motion.

2.2.5. STEP 5: Estimation of largest peak response at flexible-side frame
The largest peak response at flexible-side frame of asymmetric building model is determined from the results of the pushover analyses results described below.

1) Determine the two combined force – $\mathbf{p}_{\mathbf{U}}{}^{+}$, $\mathbf{p}_{\mathbf{U}}{}^{-}$ – from the following equation.

$$ \mathbf{p}_{\mathbf{U}}{}^{\pm} = \mathbf{M}\left(\Gamma_{1Uie}\boldsymbol{\varphi}_{\mathbf{1ie}}A_{1U\max}{}^{*} \pm 0.3\cdot\Gamma_{2Vie}\boldsymbol{\varphi}_{\mathbf{2ie}}A_{2V\max}{}^{*}\right) \tag{2.14} $$

2) Perform pushover analyses of asymmetric building model using $\mathbf{p}_{\mathbf{U}}{}^{+}$ and $\mathbf{p}_{\mathbf{U}}{}^{-}$ until the equivalent displacement at each step ${}_nD_U{}^{*}$ reaches $D_{1U}{}^{*}{}_{\max}$ obtained from STEP 2 (referred to as Pushover-1U and Pushover-2U, respectively):

$$ {}_nD_U{}^{*} = \frac{\Gamma_{1Uie}\boldsymbol{\varphi}_{\mathbf{1ie}}{}^{\mathrm{T}}\mathbf{M}_{\mathbf{n}}\mathbf{d}}{M_{1Uie}{}^{*}}, M_{1Uie}{}^{*} = \Gamma_{1Uie}{}^{2}\boldsymbol{\varphi}_{\mathbf{1ie}}{}^{\mathrm{T}}\mathbf{M}\boldsymbol{\varphi}_{\mathbf{1ie}} \tag{2.15} $$

3) Determine the largest peak response of flexible-side frame by envelope of Pushover-1U and 2U.

3. BUILDING AND GROUND MOTION DATA

3.1. Building data

The buildings considered in the present study are two four-story asymmetric buildings as shown in Fig. 3.1. The story height is 4.05m for the first story and 3.60m for the upper stories. The floor mass m_j and moment of inertia I_j are 630t and 6.01 x 10^4tm^2, respectively. The columns are assumed to be supported as fixed-ends by the foundations. The compressive strength of the concrete σ_B is assumed to be 24MPa. In addition, SD345 (yield strength: σ_y = 345MPa) is used for longitudinal reinforcement, and SD295 (σ_y = 295MPa) is used for transverse reinforcement. Each frame structure is designed according to weak-beam strong-column concept; the longitudinal reinforcements of concrete sections are determined so that the potential hinges are located at all beam-end and bottom of columns and structural wall of the first story. Sufficient shear reinforcement is assumed to be provided to prevent premature shear failure. Table 3.1 shows the dimensions and longitudinal reinforcement of each member section. The crack moment M_c and yield moment M_y of each concrete member is calculated according to AIJ Design Guideline (AIJ, 1999). The base shear coefficients obtained from the planar pushover analysis in both X- and Y-directions, which are the value when the roof displacement reaches 1% of the total height, are 0.536 (X-direction) and 0.597 (Y-direction) for Model-1, and 0.536 (X-direction) and 0.611 (Y-direction) for Model-2.

The building structure is modelled as pseudo-three dimensional frame models, in which floor diaphragms are assumed to be rigid in their own planes, there is assumed to be no out-of-plane stiffness, and the frames oriented in the X- and Y-directions are modelled independently. All columns, beams, and structural walls are modelled as one-component models with rigid zones to express the depth of intersecting members. To determine the flexibility of the nonlinear flexural springs, an

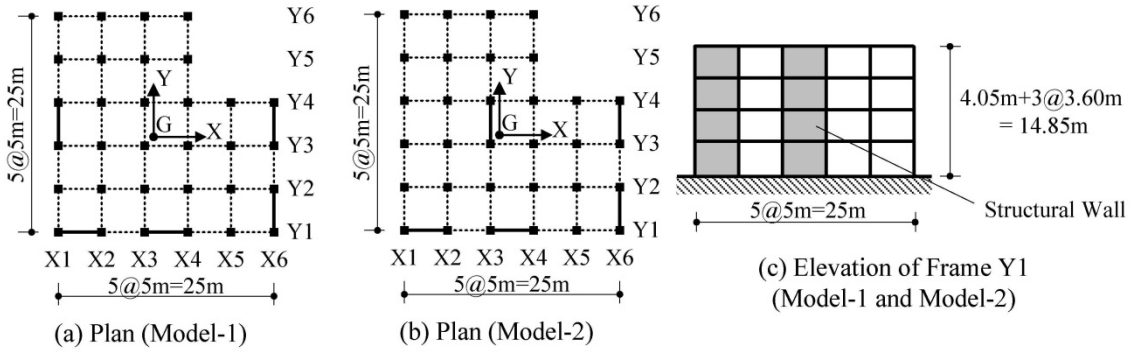

Figure 3.1 Model buildings

Table 3.1 Dimensions and longitudinal reinforcement of each member section

Member	Location	Dimension	Reinforcement
Boundary Beam	2 to R floor	350mm x 650mm	6-D25 (Top and Bottom): SD345
Beam	4 to R floor	350mm x 650mm	3-D25 (Top and Bottom): SD345
	2 to 3 floor	350mm x 650mm	4-D25 (Top and Bottom): SD345
Column	2 to 4 story	600mm x 600mm	20-D29 (Top and Bottom): SD345
	1st story	600mm x 600mm	8-D29 (Bottom), 20-D29(Top) : SD345
Structural Wall	All story	t_w = 220mm	D10@200 Double: SD295

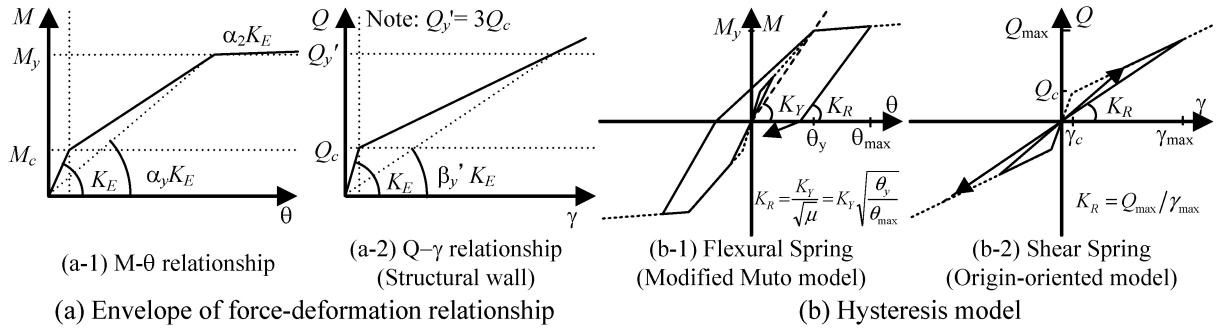

Figure 3.2 Hysteresis of nonlinear spring

anti-symmetric curvature distribution is assumed for columns and beams, whereas a uniform curvature distribution is assumed for structural walls.

Fig. 3.2(a) shows the envelope curve of force-deformation relationship of each nonlinear spring. In Fig 3.2(a-1), the secant stiffness degradation ratio of flexural spring at yield point, α_y, is assumed 0.25 for all beams and columns, while it is assumed 0.12 for the structural walls at bottom of first story and 0.19 for others. The tangent stiffness degradation ratio after yielding, α_2, is assumed 0.01 for all beams and 0.001 for all columns and structural walls. In Fig 3.2(a-2), the secant stiffness degradation ratio of shear spring at "yield point", β_y', is assumed 0.16. The axial stiffness of the columns and walls are assumed to remain elastic, and the effects of both biaxial and axial-flexural interaction are ignored. The torsional stiffness of members is also neglected. No second-order effect (e.g. P-Δ effect) is considered. The Muto hysteretic model (Muto et al., 1973) with one modification is used to model the flexural spring, as shown in Fig. 3.2(b-1). Specifically, the unloading stiffness after yielding degreases in proportion to $\mu^{-0.5}$, (μ: ductility ratio of flexural spring) to represent the degradation of unloading stiffness after yielding of R/C members, as per the model employed by Otani (Otani, 1981). The origin-oriented model (Fig. 3.2(b-2)) is used to model the shear spring of structural wall. The shear spring of beams and columns are assumed to be elastic. The damping matrix is assumed to be proportional to the instant stiffness matrix and 3% of critical damping for the elastic first mode.

Fig. 3.3 shows the *i*-th mode shapes and natural periods in elastic range T_{ie} (i = 1, 2, 3). In this figure,

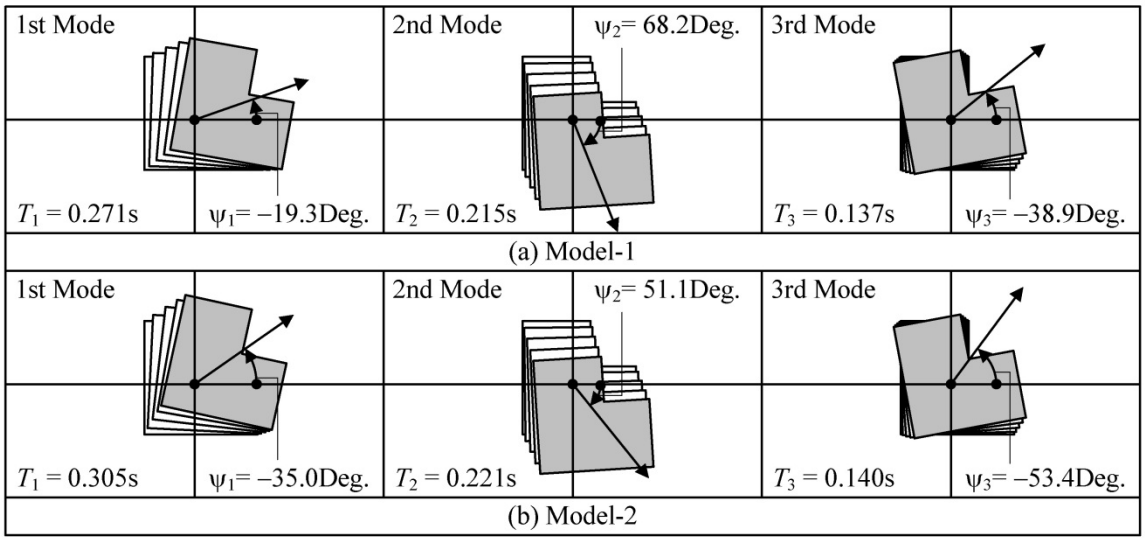

Figure 3.3 Mode shape in elastic range

the angle of incidence of principal direction of the *i*-th modal response in elastic range ψ_{ie} is also shown. As shown in this figure, the principal directions of three modes are different from the main orthogonal axes of Model-1 and 2. This figure also shows that the angle between principal axes of the first and the second modal responses is close to 90 degrees.

3.2. Ground motion data

In the present paper, the ground motion is considered bi-directional in X-Y plane, and three artificial ground motions are used. The target elastic spectrum of "major" components with 5% of critical damping $S_{A1}(T)$ is determined by Eq. (3.1) and the target elastic spectrum of "minor" component $S_{A2}(T)$ is reduced 0.7 from $S_{A1}(T)$:

$$S_{A1}(T)=\begin{cases}4.8+45T \quad \mathrm{m/s^2} & :T<0.16\mathrm{s}\\ 12.0 & :0.16\mathrm{s}\le T<0.576\mathrm{s}\\ 12.0\cdot(0.576/T) & :T\ge 0.576\mathrm{s}\end{cases} \tag{3.1}$$

In Eq. (3.1), T is the natural period of the SDOF models. The three sets of two horizontal components (first 60s of major and minor components) of the following records (El Centro 1940 (referred to as ELC), Hachinohe 1968 (HAC) and JMA Kobe 1995 (JKB)) are used to determine the phase angles of artificial ground motions. Fig. 3.4 shows the elastic acceleration spectra of artificial ground motions

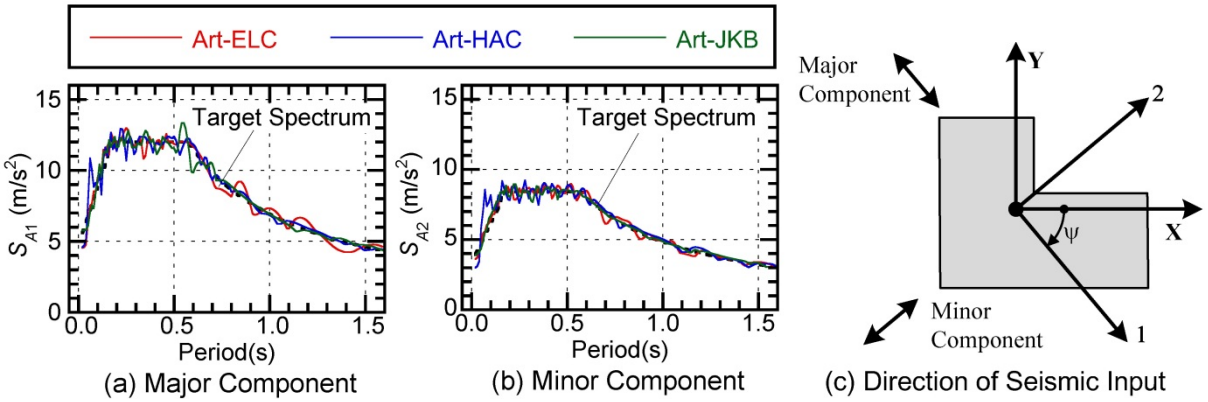

Figure 3.4 Elastic response spectra of ground motion

with 5% of critical damping. In this article, 3 x 24 = 72 cases are considered for each set of artificial ground motions; the angle of incidence of 1-axis (axis of seismic input of "major" component) varies with interval of 15 degrees from ψ_{1e} = –19.3 degrees for Model-1 and ψ_{1e} = –35.0 degrees for Model-2, respectively, and sets of artificial ground motions are scaled to 0.2, 0.6 and 1.0 so that $S_{A1}(T_{1e})$ is equal to 2.4m/s^2, 7.2m/s^2, and 12.0m/s^2, respectively.

4. ANALYSIS RESULTS AND DISCUSSIONS

4.1. Pushover analysis results and prediction of the peak response of equivalent SDOF model

Figs. 4.1 and 4.2 show the pushover analysis results of Model-1 and Model-2, respectively, prescribed in section 2.2.1 (STEP 1 of proposed procedure). In Figs 4.1(c) and 4.2(c), normalized displacement of each frame is defined as the absolute value of roof displacement of each frame divided by the equivalent displacement. For Model-1, it can be seen from Fig. 4.1(b) that the principal direction of the first modal response varies depend on $D_{1U}{}^*$; ψ_1 varies more than 30 degrees. It also can be found from Fig 4.1(c) that the larger displacement occurs at frame Y6 (X-direction) and X1 (Y-direction), respectively. Similar trend can be seen for Model-2, from Fig. 4.2, although the change of the principal direction of the first modal response is less significant in comparisons with Model-1. Since the pushover analyses results of both model show that displacement of frame Y6 and frame X1 is the largest throughout the analyses, these frames are considered as "flexible-side frames" and, attention will be paid to the response of frame Y6 and X1 in the following discussions.

Fig. 4.3 shows the estimation of seismic demand of the equivalent SDOF model in Steps 2 and 4 of the proposed procedure. In this figure, the intersection point of the capacity and demand curve represents the predicted seismic demand of the equivalent SDOF model.

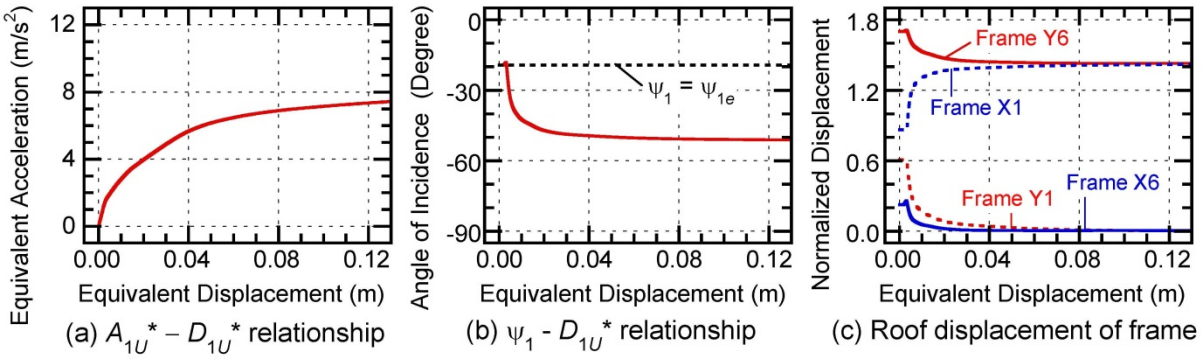

Figure 4.1 Pushover analysis results of Model-1

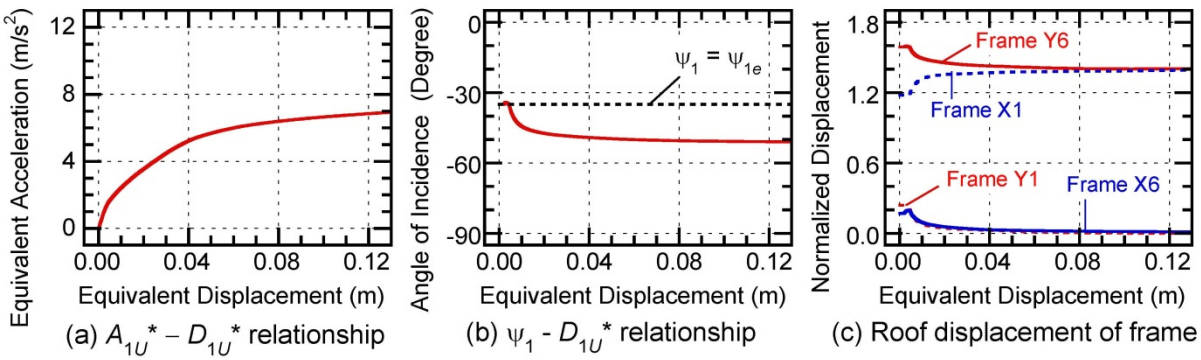

Figure 4.2 Pushover analysis results of Model-2

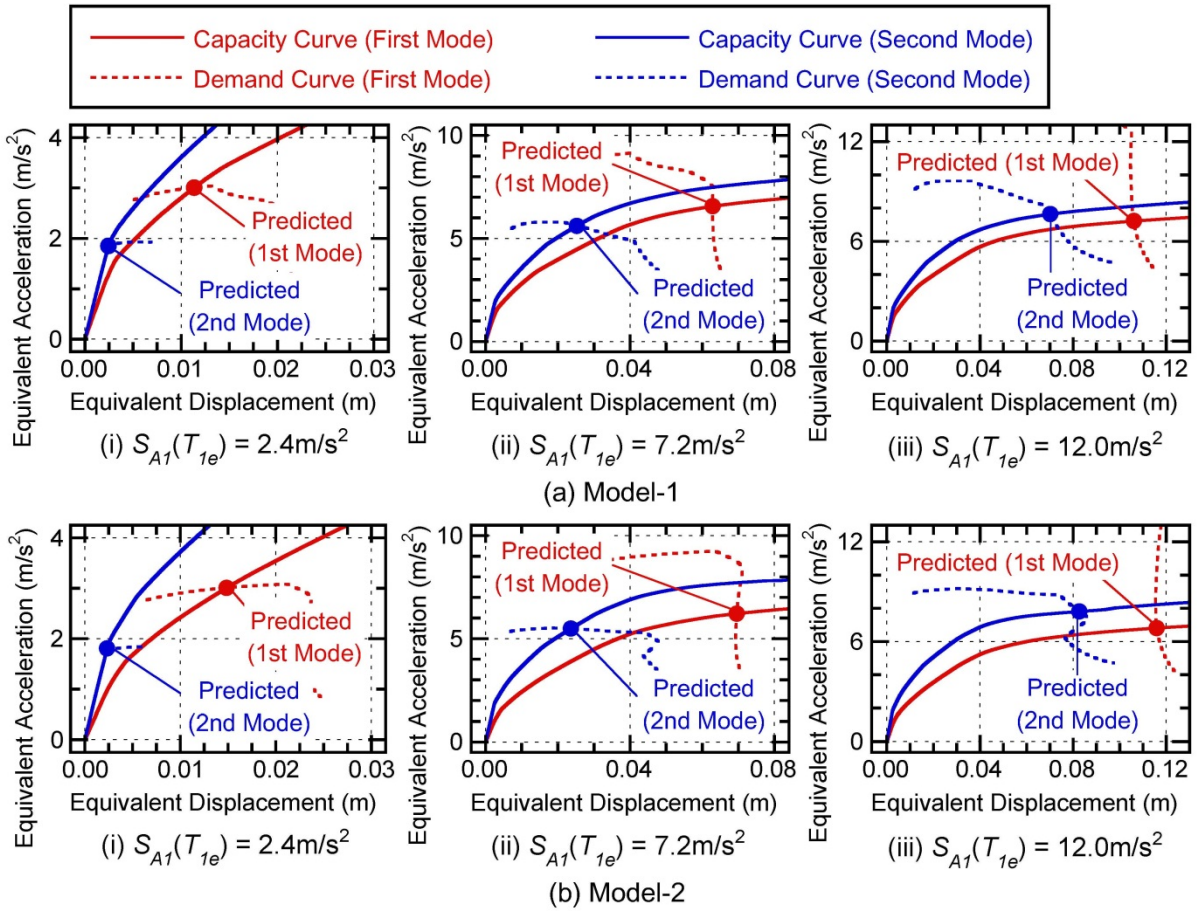

Figure 4.3 Estimation of seismic demand of equivalent SDOF models

4.2. Comparisons of predicted largest peak response with nonlinear time-history analysis results

Fig. 4.4 shows the peak of roof displacement at frames Y6 and X1 for Model-1 and Model-2, respectively, in comparisons with time-history analysis results ($S_{A1}(T_{1e})$ = 12.0m/s^2, 24 cases of various direction of seismic input) and the predicted results. As shown in this figure, the predicted result is well agreed with the upper bound of peak roof displacement obtained from time-history analyses results. Fig 4.5 shows the largest peak drift at frame Y6 and X1 for both models, in comparisons with time-history analysis results (the maximum of 24 cases for each set of ground motions) and the predicted results. As shown in this figure, the predicted results agree with the results of the time-history analysis results.

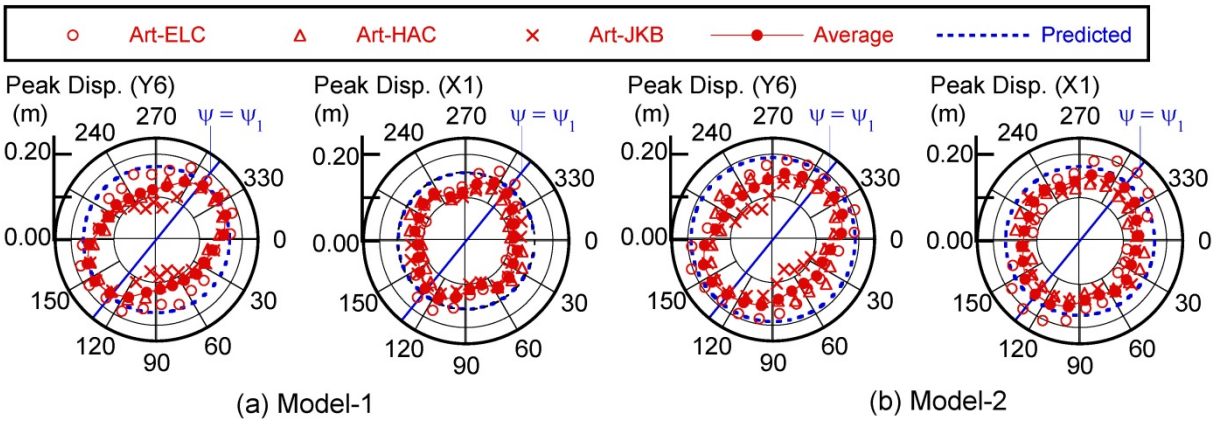

Figure 4.4 Prediction of the largest peak roof response at flexible-side frames

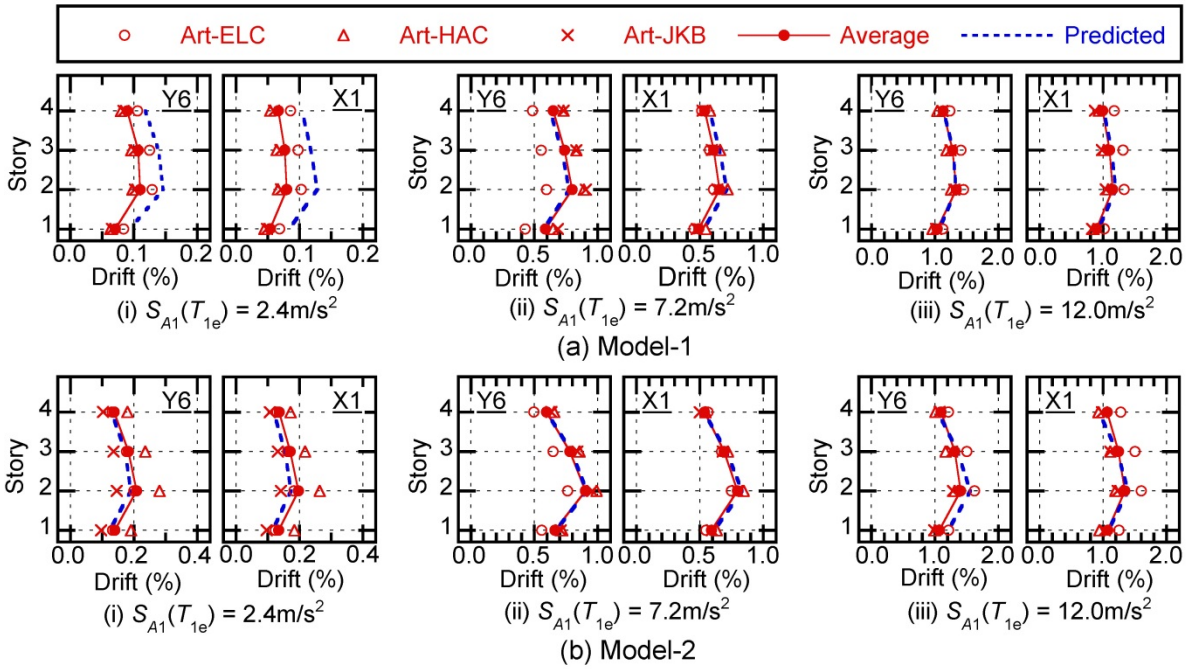

Figure 4.5 Comparisons of the largest peak response at flexible-side frames

5. CONCLUSIONS

In this present article, the modified procedure to predict the largest peak seismic response at flexible-side frame of asymmetric building considering horizontal bi-directional ground motion act in arbitrary angle of incidence is proposed. The results show the largest peak response at flexible-side frame can be satisfactorily predicted by the proposed procedure.

AKCNOWLEDGEMENT

The author acknowledges support by Grant-in-Aid for Young Scientist (Category (B), No. 21760443), Japan Ministry of Education, Culture, Sport, Science and Technology (MEXT).

REFERENCES

Vanvasikos, D., Cornell, C. A. (2001). Incremental dynamic analyisis. *Earthquake Engineering and Structural Dynamics*. **31:** 491-514.

Dolšek, M., Fajfar P. (2007). Simplified probabilistic seismic performance assessment of plan-asymmetric buildings. *Eartquake Engineering and Structural Dynamics*. **36:13**, 2021-2041.

Fujii, K. (2010). Seismic Assessment of Asymmetric Buildings Considering the Critical Direction of Seismic Input. *14th European Conference on Earthquake Engineering*, Paper No. 0623.

Fujii, K. (2011). Nonlinear static procedure for multi-story asymmetric frame buildings considering bi-directional excitation. *Journal of Earthquake Engineering*. **15**, 245-273.

Otani, S. (2000) New seismic design provision in Japan. *The Second U.S.-Japan Work-shop on Performance-Based Earthquake Engineering Methodology for Reinforced Concrete Structures*, PEER Report 2000/10, 3-14.

Architectural Institute of Japan (AIJ). (1999). Design Guidelines for Earthquake Resistant Reinforced Concrete Buildings Based on Inelastic Displacement Concept. Architectural Institute of Japan, Tokyo (in *Japanese*).

Muto, K., Hisada, T., Tsugawa, T., and Bessho, S. (1973), Earthquake Resistant Design of a 20 Story Reinforced Concrete Buildings. *Proceedings of the 5th World Conference on Earthquake Engineering*, 1960-1969.

Otani, S. (1981), Hysteresis Models of Reinforced Concrete for Earthquake Response Analysis. *Journal, Faculty of Engineering, University of Tokyo*. **36:2**, 125-156.